

## Degradation Processes of the Single-Crystal Silicon Electrodes during lithiation

*E.Yu. Evshchik<sup>1</sup>, A.V. Korchun<sup>1</sup>, A.V. Levchenko<sup>1</sup>, Y.A. Dobrovolsky<sup>1,2</sup>*

<sup>1</sup> Institute of Problems of Chemical Physics, Russian Academy of Sciences, Chernogolovka 142432, Moscow Region, Russia

<sup>2</sup> Platov South-Russian State Polytechnic University (NPI), Novocherkassk 346428, Rostov Region, Russia

\*E-mail: [liza@icp.ac.ru](mailto:liza@icp.ac.ru)

*Received: 23 September 2020 / Accepted: 2 November 2020 / Published: 30 November 2020*

---

The influence of crystal lattice orientation on lithiation process of *p*-type single-crystal silicon was investigated using cyclic voltammetry, galvanostatic cycling and electronic impedance spectroscopy. The surfaces of electrodes following cycling were studied using scanning electron microscopy. Defects formed during 100 charge-discharge cycles as a result of partial electrode destruction ranges from 50 to 100 nm, accounting for the cycling stability of electrodes based on silicon nanoparticles of sizes not exceeding 150 nm.

---

**Keywords:** Lithium-ion battery, single-crystal silicon, anode material, electrode capacity

### 1. INTRODUCTION

The specific energy of modern lithium-ion batteries (LIB) is currently insufficient to provide the desired autonomy of portable devices and electric vehicles. A significant improvement in the mass and size characteristics of the batteries can be achieved by increasing the capacity of at least one of the electrodes. This can be implemented by replacing graphite in the negative LIB electrode with a silicon-based material, by which means electrode capacity can theoretically be increased by up to 10 times.

The chief obstacle to the use of silicon as the main component of the negative electrode of LIB is the degradation of this material during reversible lithiation, which is due to significant changes in volume and processes occurring at the interface of the electrode [1-4]. Therefore, an important task in the development of stable silicon-based electrodes is to determine the mechanism of degradation processes and identify the main factors affecting these processes. The obtained information will make it possible to minimise irreversible capacity losses and ensure the long-term performance of silicon

anodes. Single-crystal silicon can be used as a model system for studying silicon lithiation processes and estimating the size of defects arising during delithiation [5, 6]. This will help to validate the optimal particle size to prevent significant degradation of the silicon-based anode material upon cycling.

The electrochemical insertion of Li into crystalline Si results in the formation of  $\text{Li}_x\text{Si}$  intermetallic compounds [1-4]. The reaction proceeds along the phase boundary between crystalline and lithiated silicon [7-11]. During the formation of silicides, a significant increase in the volume and plastic deformation of the material occurs. The structural changes on the surface during cycling and insertion/extraction of lithium depend on the orientation of the silicon crystal lattice [12-27], as well as the presence of additives (dopants) that improve the conductivity of the material [28-31]. Along with the appearance of defects, the deformation of the surface of a single Si crystal is directly dependent on the orientation of the silicon crystal lattice [8, 9, 11, 20]. Silicon has a low conductivity, which can be increased by using conductive additives, for example, phosphorus (electronic conductivity, *n*-Si) or boron (hole conductivity, *p*-Si) [28-30]. The type and density of such doping can affect the structural changes, phase transformations and interstitial extraction processes of lithium into nanosized silicon [18].

The present work is devoted to the study of the surface degradation of a single-crystal silicon electrode using samples doped with boron (*p*-type conductivity) having crystal lattice orientations (100) and (111). For *p*-type silicon, the rate of interfacial insertion of lithium is low compared to that of *n*-type silicon, which allows a more detailed investigation of the processes of reversible Si lithiation [30]. In our experiments, multiple insertion/extraction of lithium covered the designed depth of 1  $\mu\text{m}$  from the surface of the single Si crystal. The influence of crystal lattice orientation on the electrochemical characteristics of the Si electrode was revealed along with resulting changes in surface morphology.

## 2. EXPERIMENTAL

### 2.1. Materials

Plates of boron-doped single-crystal silicon with crystal lattice orientation (111) and (100) (OSTEK, Russia) were used as electrodes. The size and thickness of the electrodes were 1.5 x 1.5  $\text{cm}^2$  and 200  $\mu\text{m}$ , respectively. To ensure good contact with the current collector, a Ti sublayer with a thickness of 50 nm and a Cu layer with a thickness of 250 nm were deposited on one side of the single crystal surface, according to the technique described in [32]. Copper foil tightly pressed against the sample was used as a current collector.

### 2.2. Electrochemical measurements

For electrochemical measurements, three-electrode tightly-assembled Teflon cells were used. These cells were specially produced within an argon-filled glove box. The counter electrode and

reference electrode were made of lithium foil pressed onto a copper current collector. The electrodes were isolated by a 25  $\mu\text{m}$  thick polypropylene separator PORP (Ufim, Russia). 1M  $\text{LiPF}_6$  in a mixture of ethylene carbonate and diethyl carbonate mixture (1:1, vol.) (Aldrich, battery grade) served as an electrolyte.

A cyclic voltammogram (CV) in the potential range of 0.4-2.0 V was taken prior to galvanostatic cycling in order to activate a sample surface; the scan rate was 0.1 mV/s.

Lithium insertion and extraction processes were studied by means of galvanostatic cycling using a P-20X80 multichannel potentiostat (Elins, Russia). During cycling with a current density of 50  $\text{mA}/\text{cm}^2$ , the insertion of  $\text{Li}^+$  was interrupted when reaching a pre-calculated charge level (see Section 3), while extraction was ended at 2V.

Electrochemical impedance spectra were recorded on a Z-1500 P analyser (Elins, Russia) within an AC frequency range of 0.01 Hz–10 kHz having potential amplitude of 10 mV.

### 2.3. Morphology characterisation

The surfaces of the silicon electrodes following cycling were examined using a scanning electron microscope (Zeiss LEO SUPRA 25, Germany).

## 3. RESULTS AND DISCUSSION

During the preliminary galvanostatic cycling of Si samples at 50  $\text{mA}/\text{cm}^2$ , no lithium insertion/extraction processes were observed regardless of the orientation of the Si crystal lattice and the resistance of the sample. Therefore, in subsequent experiments, a scan of the cyclic voltammogram (CV) was taken prior to commencing the cycling procedure in order to activate the sample surface.

Fig. 1 presents cyclic voltammograms for single-crystal silicon electrodes having different crystal lattice orientations. Here it can be seen that the CV curves for both Si samples have a similar appearance, demonstrating cathodic (reflecting the formation of  $\text{Li}_x\text{Si}$  compounds) and anodic (reflecting the decomposition of  $\text{Li}_x\text{Si}$  compounds) current peaks. The CV results demonstrate that, in both cases, the lithiation of single-crystal silicon begins at 0.12 V during the first cycle. However, during the second cycle, since the electrode surface was no longer single-crystal, the cathodic peaks corresponding to lithium insertion shifted toward a higher potential of 0.3 V. The two anodic peaks visible at potentials 0.35 and 0.53 V are associated with the decomposition of lithium silicides  $\text{Li}_x\text{Si}$  [33-35]. A sharp increase in the peak intensities in the 2nd cycle (Fig. 1) can be explained in terms of an increase in the fraction of the silicon crystal's electrochemically active surface.

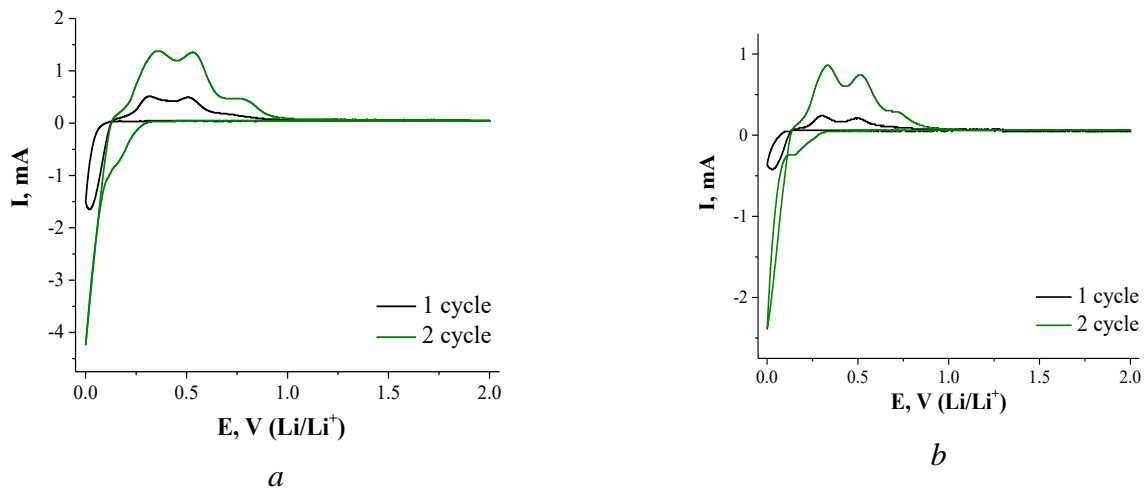


**Figure 1.** Cyclic voltammograms of single-crystal silicon with crystal lattice orientations (111) (a) and (100) (b) (scan rate 0.1 mV/s)

According to the literature data [36], the process of silicon lithiation is similar to those of an oxide layer formation on the Si surface. At the initial cycling stage, the increase in lithium content is controlled by the rate of the lithiation reaction [37]. Due to the current density increasing during the cycling, both the depth of the lithiation and the time required to transfer lithium from the surface to the depth of the Si single crystal increase.

The intensity of the peaks for the second cycle increases significantly for both samples. The maximum current for the sample with crystal lattice orientation (111) in the anodic region is 1.4 mA, while in the cathodic region the maximum current is 4.2 mA; this is almost two times higher than the respective currents of the sample having crystal lattice orientation (100) (Fig. 1). Consequently, at the initial stage of cycling, the surface with crystal lattice orientation (111) is more active towards lithium insertion, which observation is quite consistent with the literature data. The increase of the peak intensity can be explained by an increase in the electrochemically-active surface area of the silicon crystal.

At the initial stage of single-crystal silicon lithiation, amorphisation of its working surface occurs through the formation of lithiated amorphous silicides  $\text{Li}_x\text{Si}$  [38]. In the amorphous  $\text{Li}_x\text{Si}$ , the value  $x$  varies within the range  $0 < x < 3.75$  [39, 40]. According to [41], there are two amorphous phases:  $\text{Li}_{2.1}\text{Si}$  and  $\text{Li}_{3.3}\text{Si}$ . Diffusion of lithium into these phases occurs rather quickly and deeply through structural defects, up to pure silicon.

Following preliminary activation through two cycles of CV, galvanostatic charge-discharge with a current of  $50 \mu\text{A}/\text{cm}^2$  was carried out.

According to literature data, the amorphous  $\text{Li}_x\text{Si}$  phase is recrystallised at potentials less than 50 mV to form metastable  $\text{Li}_{15}\text{Si}_4$  [42-45] resulting in deep lithiation. The theoretical capacity of the resulting compound is 3579 mAh/g. The resulting phase is unstable and very active, which can manifest itself in the self-discharge of an electrode during chemical reaction with an electrolyte [46]. During delithiation, amorphous silicon is formed from the  $\text{Li}_{15}\text{Si}_4$  phase according to the two-phase

mechanism [42]. In order to prevent deep degradation of the electrode and study the surface of the electrodes following cycling, the insertion of lithium into single-crystal silicon was carried out up to a designed depth of 1  $\mu\text{m}$ . Calculations of the necessary electric charge were performed based on relations (1-4) and the resulting formula (5):



$$n(\text{Si}) = 4n(\text{Li}) \quad (2)$$

$$n(\text{Si}) = \frac{h \cdot S \cdot \rho}{M} \quad (3)$$

$$n(\text{Li}) = \frac{n(\text{Si})}{4} \quad (4)$$

$$Q = n(\text{Li}) \cdot F \quad (5)$$

(here  $h$  – depth of lithium insertion, cm;  $S$  – electrode area,  $\text{cm}^2$ ;  $\rho$  – density of silicon ( $2.3 \text{ g/cm}^3$ );  $M$  – molar mass of silicon ( $28 \text{ g/mol}$ );  $F$  – Faraday constant ( $96485 \text{ C/mol}$ )).

In order to analyse the processes occurring on the charged electrode and compare the data obtained for samples with different crystal lattice orientations, the electrochemical impedance spectra of charged and discharged electrodes were recorded. It was established that the electrode resistance is practically independent of the orientation of the silicon crystal lattice. The impedance of both samples under investigation contains three main components: electrolyte resistance, Faraday impedance and diffusion impedance (Fig. 2).

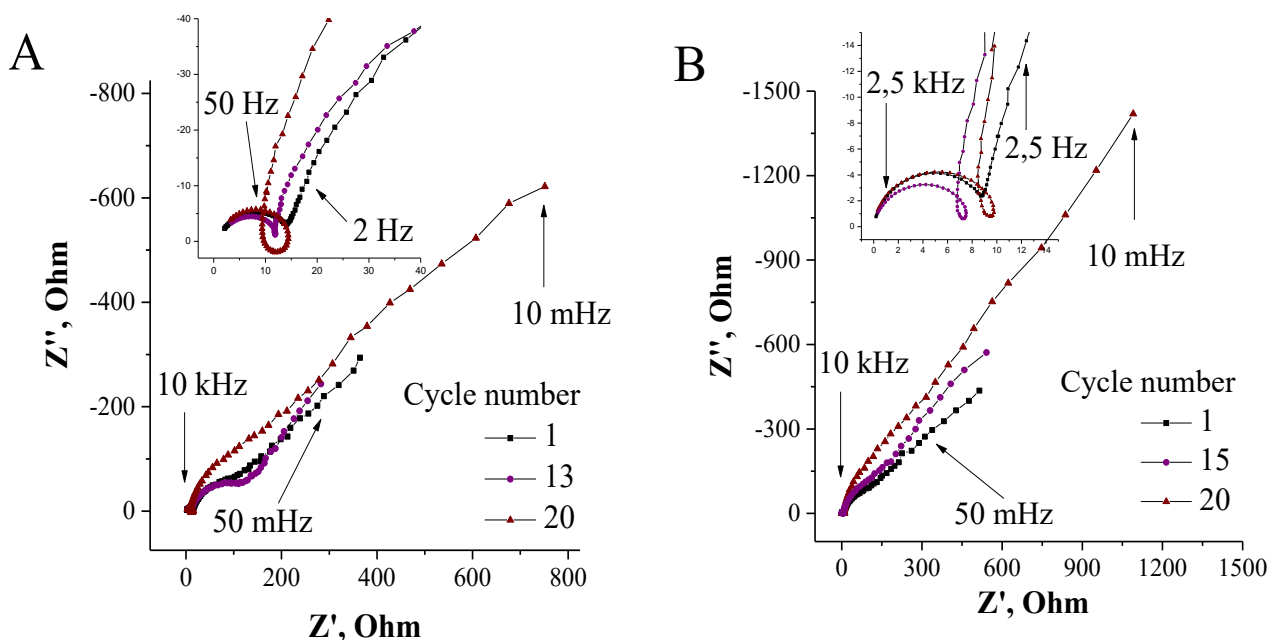


**Figure 2.** Impedance spectra of charged electrodes with crystal lattice orientation (111) (a) and (100) (b) (high-frequency spectra on the insets)

On the 14<sup>th</sup> charge cycle, the electrodes demonstrated an inductive-like feature, which became more pronounced as the number of cycles increased. This phenomenon can be associated with the formation of a developed silicon surface during its destruction, on which an unstable solid electrolyte interface (SEI) is formed. The lithium-containing compounds appeared during the formation of SEI as a result of the interaction of lithium with silicon. In this case, chemical decomposition of the sample surface results in changes in the activity of electrochemically active components in the near-electrode layer, leading to the appearance of an inductive-like feature.

At the 16<sup>th</sup> cycle for the Si (100) sample and the 20<sup>th</sup> cycle for the Si (111) sample, there is a sharp increase in electrode resistance associated with the delamination of silicon particles. The destruction of the surface of the electrode based on Si (111) occurs more slowly, since in this case the lithiation rate is lower than for the Si (100) electrode [9, 11, 21, 47].

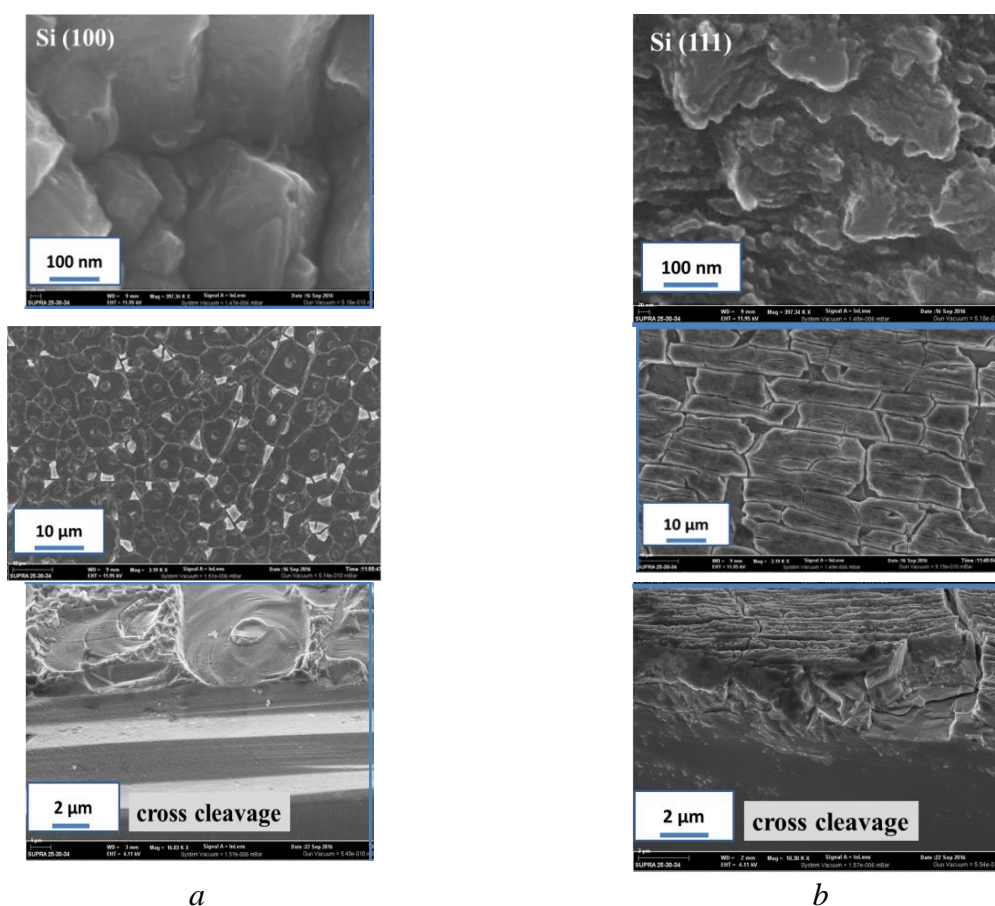


**Figure 3.** SEM images of Si monocrystal electrodes with crystal lattice orientation (100) (a) and (111) (b) after 25 cycles

Nevertheless, the intensity of the Si (111) peaks in the cyclic voltammograms is higher than that of Si (100) (Fig. 1). This may be due to the processes that occur during the activation stage: the surface of the Si (111) sample is destroyed faster, after which the structure is stabilised, leading to a decrease in the lithiation rate. For electrodes based on both Si (100) and Si (111), after 12-13

galvanostatic charge-discharge cycles, irreversible changes in the structure of the surface were noted. Such behaviour can be attributed to the destruction of contact between silicon particles.

To determine average particle size on the surface of the electrodes, SEM-images were made after 25 (for Si (111) and Si (100)) and 100 (for Si (100)) charge-discharge cycles at 50 mA/cm<sup>2</sup>. Microscopic studies of the samples following 25 charge-discharge cycles showed that the morphology of silicon particles is significantly determined by the orientation of the crystal lattice (Fig. 3), which is consistent with the literature data [33].

During lithiation, defects are formed on the surface, with amorphization occurring on a layer-by-layer basis [21]. Upon lithiation (100), cracks are observed on the surface of the single crystal, while complex vein-like microstructures of Li<sub>x</sub>Si are formed in the crystalline silicon matrix; however, some areas retain the original structure. The formation of the crystalline phase of Li<sub>15</sub>Si<sub>4</sub> in the (100) samples can cause localised tensile stresses, which lead to surface cracking and an increase in the rate of diffusion of lithium into silicon. As it was shown in [20], in the bulk of lithiated silicon (100), there is a network consisting of Li<sub>x</sub>Si layers with a thickness of the order of several hundred nanometres, penetrating into the depth of the wafer surface by ~ 6 μm.

Fig. 4 provides a SEM image of Si (100) electrode surface after 100 charge-discharge cycles to a calculated depth of 1 μm.

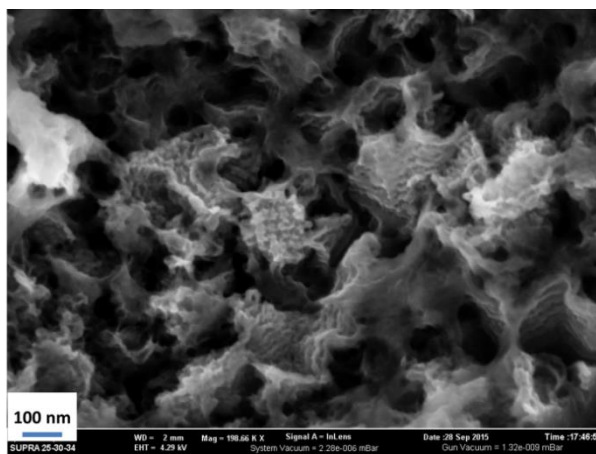


**Figure 4.** SEM image of Si (100) electrode after 100 cycles (designed lithiation depth of 1 μm)

The results demonstrate that the characteristic size of fragments that are not destroyed due to prolonged insertion-extraction of lithium into silicon is ~ 50–150 nm. This explains the cycling stability of crystalline silicon nanomaterials less than 150 nm in size [1, 48-51].

#### 4. CONCLUSION

The orientation of the crystal lattice does not influence the initial lithiation potential of single-crystal silicon: the process begins at a potential of ~ 0.12 V for both Si (111) and Si (100) electrodes.

However, at the initial stage of cycling, the surface of Si (111) is more active against lithium than the surface of Si (100). Upon cycling, the resistance of charged and discharged electrodes is practically independent of the orientation of the crystal lattice. The characteristic size of fragments formed on the surface of the single silicon crystal following 100 charge-discharge cycles as a result of its partial destruction ranges from 50 to 100 nm. This helps to account for the well-attested cycling stability of electrodes based on silicon nanoparticles having a size not exceeding 150 nm.

#### ACKNOWLEDGEMENTS

This work was performed with financial support from Ministry of Science and Higher Education of Russian Federation, project ID RFMEFI60419X0235.

#### References

1. M.N. Obrovac, V.L. Chevrier, *Chem. Rev.*, 114 (2014) 11444.
2. J.-Y. Li, Q. Xu, G. Li, Y.-X. Yin, L.-J. Wan, Y.-G. Guo, *Mater. Chem. Front.*, 1 (2017) 1691.
3. M. Ashuri, Q. Hea, L.L. Shaw, *Nanoscale*, 8 (2016) 74.
4. X. Su, Q. Wu, J. Li, X. Xiao, A. Lott, W. Lu, B.W. Sheldon, J. Wu, *Adv. Energy Mater.*, 4 (2014) 1300882.
5. H.R. Yao, Z.Q. Wang, M.S. Wu, G. Liu, X.L. Lei, B. Xu, J.X. Le, C.Y. Ouyang, *Int. J. Electrochem. Sci.*, 9 (2014) 1854.
6. J. Huang, Z. Wang, X. Gong, M. Wu, G. Liu, X. Lei, J. Liang, H. Cao, F. Tang, M. Lei, B. Xu, C. Ouyang, *Int. J. Electrochem. Sci.*, 8 (2013) 5643.
7. X.R. Liu, H.J. Yan, D. Wang, L.J. Wan, *Acta Phys. -Chim. Sin.*, 32 (2016) 283.
8. M. Song, S.P.V. Nadimpalli, V.A. Sethuraman, M.J. Chon, P.R. Guduru, L.Q. Wang, *J. Electrochem. Soc.*, 161 (2014) 915.
9. M. Pharr, K. Zhao, X. Wang, Z. Suo, J.J. Vlassak, *Nano Lett.*, 12 (2012) 5039.
10. X.H. Liu, J.W. Wang, S. Huang, F. Fan, X. Huang, Y. Liu, S. Krylyuk, J. Yoo, S.A. Dayeh, A.V. Davydov, S.X. Mao, S.T. Picraux, S. Zhang, J. Li, T. Zhu, J.Y. Huang, *Nat. Commun.*, 7 (2012) 749.
11. M.J. Chon, V.A. Sethuraman, A. McCormick, V. Srinivasan, P.R. Guduru, *Phys. Rev. Lett.*, 107 (2011) 0455031.
12. X.H. Liu, H. Zheng, L. Zhong, S. Huang, K. Karki, L.Q. Zhang, Y. Liu, A. Kushima, W.T. Liang, J.W. Wang, J.-H. Cho, E. Epstein, S.A. Dayeh, S.T. Picraux, T. Zhu, J. Li, J.P. Sullivan, J. Cumings, C. Wang, S.X. Mao, Z.Z. Ye, S. Zhang, J.Y. Huang, *Nano Lett.*, 11 (2011) 3312.
13. Y.-J. Ko, K.J. Chang, *Phys. Rev. B*, 56 (1997) 9575.
14. S.C. Jung, Y.K. Han, *Phys. Chem. Chem. Phys.*, 13 (2011) 21282.
15. K. Zhao, M. Pharr, Q. Wan, W.L. Wang, E. Kaxiras, J.J. Vlassak, Z. Suo, *J. Electrochem. Soc.*, 159 (2012) 238.
16. H. Yang, S. Huang, X. Huang, F.F. Fan, W.T. Liang, X.H. Liu, L.Q. Chen, J.Y. Huang, J. Li, T. Zhu, S.L. Zhang, *Nano Lett.*, 12 (2012) 1953.
17. J.F. Nye, *Physical Properties of Crystals*, Clarendon Press, (1985) Oxford, Great Britain.
18. B. Peng, F.Y. Cheng, Z.L. Tao, J. Chen, *J. Chem. Phys.*, 133 (2010) 034701.
19. M.K.Y. Chan, C. Wolverton, J.P. Greeley, *J. Am. Chem. Soc.*, 134 (2012) 14362.
20. Y.S. Choi, M. Pharr, C.S. Kang, S.B. Son, S.C. Kim, K.B. Kim, H. Roh, S.H. Lee, K.H. Oh, J.J. Vlassak, *J. Power Sources*, 265 (2014) 160.
21. C.S. Kang, S.B. Son, J.W. Kim, S.C. Kim, Y.S. Choi, J.Y. Heo, S.S. Suh, Y.U. Kim, Y.Y. Chu, J.S. Cho, S.H. Lee, K.H. Oh, *J. Power Sources*, 267 (2014) 739.

22. S.W. Lee, M.T. McDowell, L.A. Berla, D. Nix, Y. Cui, *Proc. Natl. Acad. Sci. U.S.A*, 109 (2012) 4080.
23. Q. Zhang, Y. Cui, E. Wang, *J. Phys. Chem. C*, 115 (2011) 9376.
24. J.L Goldman, B.R. Long, A.A. Gewirth, R.G. Nuzzo, *Adv. Funct. Mater.*, 21 (2011) 2412.
25. J. Li, J.R. Dahn, *J. Electrochem. Soc.*, 154 (2007) 156.
26. K.J. Zhao, A.G. Tritsarlis, M. Pharr, W.L. Wang, O. Okeke, Z.G. Suo, J.J. Vlassak, E. Kaxiras, *Nano Lett.*, 12 (2012) 4397.
27. W.H. Wan, Q.F. Zhang, Y. Cui, E.G. Wang, *J. Phys.: Condens. Matter.*, 22 (2010) 4155011.
28. J. Antula, B.F. Becker, *J. Phys. Chem.*, 79 (1975) 2470.
29. B.R. Long, M.K.Y. Chan, J.P. Greeley, A.A. Gewirth, *J. Phys. Chem. C*, 115 (2011) 18916.
30. W. McSweeney, O. Lotty, C. Glynn, H. Geaney, J. D. Holmes, C. O'Dwyer, *Electrochim. Acta*, 135 (2014) 356.
31. C.K. Chan, H. Peng, G. Liu, K. McIlwrath, X.F. Zhang, Y. Cui, *Nat. Nanotechnol.*, 3 (2008) 31.
32. V.A. Sethuraman, M.J. Chon, M. Shimshak, V. Srinivasan, P.R. Guduru, *J. Power Sources*, 195 (2010) 5062.
33. M. Green, E. Fielder, B. Scrosati, M. Wachtler, J.S. Moreno, *Electrochem. Solid-State Lett.*, 6 (2003) 75.
34. B.R. Long, M.K.Y. Chan, J.P. Greeley, A.A. Gewirth, *J. Phys. Chem. C*, 115 (2011) 18916.
35. K.W. Schroder, H. Celio, L.J. Webb, K.J. Stevenson, *J. Phys. Chem. C*, 116 (2012) 19737.
36. B.E. Deal, A.S. Grove, *J. Appl. Phys.*, 36 (1965) 3770.
37. F. Shi, Z. Song, P.N. Ross, G.A. Somorjai, R.O. Ritchie, K. Komvopoulos, *Nat. Commun.*, 7 (2016) 11886.
38. P. Limthongkul, Y.-I. Jang, N.J. Dudney, Y.-M. Chiang, *J. Power Sources*, 119 (2003) 604.
39. M. Gu, Y. He, J. Zheng, C. Wang, *Nano Energy*, 17 (2015) 366.
40. K. Ogata, E. Salager, C.J. Kerr, A.E. Fraser, C. Ducati, A.J. Morris, S. Hofmann, C.P. Grey, *Nat. Commun.*, 5 (2014) 3217.
41. N. Ding, J. Xu, Y.X. Yao, G. Wegner, X. Fang, C.H. Chen, I. Lieberwirth, *Solid State Ionics*, 180 (2009) 222.
42. M.N. Obrovacz, L. Christensen, *Electrochem. Solid-State Lett.*, 7 (2004) 93.
43. X.H. Liu, L.Q. Zhang, L. Zhong, Y. Liu, H. Zheng, J.W. Wang, J.-H. Cho, S.A. Dayeh, S.T. Picraux, J.P. Sullivan, S.X. Mao, Z.Z. Ye, J.Y. Huang, *Nano Lett.*, 11 (2011) 2251.
44. C.-M. Wang, X. Li, Z. Wang, W. Xu, J. Liu, F. Gao, L. Kovarik, J.-G. Zhang, J. Howe, D.J. Burton, Z. Liu, X. Xiao, S. Thevuthasan, D.R. Baer, *Nano Lett.*, 12 (2012) 1624.
45. M. Gu, Z. Wang, J.G. Connell, D.E. Perea, L.J. Lauhon, F. Gao, C. Wang, *ACS Nano*, 7 (2013) 6303.
46. B. Key, R. Bhattacharyya, M. Morcrette, V. Seznec, J.-M. Tarascon, C.P. Grey, *J. Am. Chem. Soc.*, 131 (2009) 9239.
47. N. Aoki, A. Omachi, K. Uosaki, T. Kondo, *ChemElectroChem*, 3 (2016) 959.
48. H. Kim, M. Seo, M.H. Park, J. Cho, *Angew. Chem. Int. Ed.*, 49 (2010) 2146.
49. H. Ghassemi, M. Au, N. Chen, P.A. Heiden, R.S. Yassar, *ACS Nano*, 5 (2011) 7805.
50. J.R. Heath, *Science*, 258 (1992) 1131.
51. H.Li, X. Haung, L. Chen, Z. Wu, Y. Liang, *Electrochem. Solid-State Lett.*, 2 (1999) 547.